Xuan, T.; Pastor, JV.; García-Oliver, JM.; García Martínez, A.; He, Z.; Wang, Q.; Reyes, M. (2019). In-flame soot quantification of diesel sprays under sooting/non-sooting critical conditions in an optical engine. Applied Thermal Engineering. 149:1-10. https://doi.org/10.1016/j.applthermaleng.2018.11.112

In-flame soot quantification of Diesel sprays under sooting/non-sooting critical conditions in an optical engine

Tiemin Xuan[1], José V. Pastor[2], José María García-Oliver[2], Antonio García[2], Zhixia He[3*], Qian Wang[1*], Miriam Reyes[4]

1 School of Energy and Power Engineering, Jiangsu University, Zhenjiang 212013, China

2 CMT-Motores Térmicos, Universitat Politècnica de València, Valencia 46022, Spain

3 Institute for Energy Research, Jiangsu University, Zhenjiang 212013, China

4 Department of Energy and Fluid Mechanics Engineering, University of Valladolid, Paseo del Cauce s/n, E-47011, Valladolid, Spain

*** Corresponding author:**

Zhixia He, Institute for Energy Research, Jiangsu University, No.301, Xuefu Road, Zhenjiang, 212013, China
Tel: +86 13776476205 Email: zxhe@ujs.edu.cn

Qian Wang, School of Energy and Power Engineering, Jiangsu University, No.301, Xuefu Road, Zhenjiang, 212013, China Tel: +86 13912802056 Email: qwang@ujs.edu.cn

Abstract

Because of the challenge of meeting stringent emissions regulations for internal combustion engines, some advanced low temperature combustion modes have been raised in recent decades to improve combustion efficiency. Therefore, detailed understanding and capability for accurate prediction of in-flame soot processes under such low sooting conditions are becoming necessary. Nowadays, a lot of investigations have been carried out to quantify in-flame soot in Diesel sprays under high sooting conditions by means of different optical techniques. However, no information of soot quantification can be found for sooting/non-sooting critical conditions. In current study, the instantaneous soot production in a two-stroke optical engine under low sooting conditions has been measured by means of a Diffused back-illumination extinction technique (DBI) and two-color method (2C) simultaneously. The fuels used were n-dodecane and n-heptane, which have been injected separately though two different injectors equipped with single-hole nozzles. A large cycle-to-cycle variation on soot production can be observed under such operating conditions, however the in-cylinder heat release traces were quite repeatable. It is the same with the well-known trends of soot amount to operating conditions that the probability of sooting cycles increases with higher ambient temperature, higher ambient density and lower injection pressure. Both techniques present a pretty good agreement on soot amount when the peak of KL value is close to 1. However, the KL value of two-color method becomes bigger than that of DBI and the difference increases with lower sooting conditions.

Keywords: Diesel sprays; soot critical conditions; optical engine; DBI; 2C

Highlights:

- One criterium based on radiation images has been defined to quantify sooting /non-sooting cycles.
- Lift-off length variation has been found as the main reason of strong cycle-to-cycle soot variations.

- DBI and Two-color method have been applied simultaneously under such sooting/non-sooting critical conditions.
- The advantages and limitations of both techniques have been compared.

Nomenclature

CFD	computational fluid dynamics
HTHP	high-temperature high-pressure
DBI	diffused back-illumination (DBI) extinction imaging
2C	two-color method
KL	optical thickness
KL_I	optical thickness from DBI technique
KL_{2C}	optical thickness from two-color method
I_f	flame intensity
I_0	background intensity
I_t	transmitted intensity
I_b	black body intensity
LOL	lift-off Length (mm)
ASOI	after the start of injection (μs)
ASOE	after start of energizing (μs)
P_{inj}	injection pressure (bar)
T_a	ambient gas temperature (K)
d_0	orifice diameter
HT	high temperature conditions
MT	medium temperature conditions
LT	low temperature conditions

Greek symbols

ρ_a	ambient density
ρ_f	fuel density
ε	emissivity
λ	wavelength (nm)
τ	transmissivity
$\overline{\Phi}_H$	cross-sectional average equivalence ratio at flame lift-off length
θ	jet spreading angle.

1 Introduction

Compression-ignition (CI) engines have been widely used as the power machinery for vehicles because of their high-power performance, low fuel consumption. However, soot emissions formed in the combustion of CI engines have significant negative impacts on human health and environment. Therefore, it is quite necessary for engine researchers to have more knowledge on soot production process and to reduce soot emission. Because of the extremely complex interaction between numerous physical and chemical processes involved in soot formation and oxidation, it is still a big

challenge for CFD to predict in-flame soot characteristics precisely [1]. In recent years, in order to have a better understanding of the soot processes in diesel combustion, lots of optical diagnostics have been applied in two main types of facilities, namely optical engines [1]-[8] and high-temperature high-pressure vessels (HTHP) [9]-[15]. In the latter type of facilities, the boundary conditions are highly controlled and injections are performed in a nearly quiescent environment. Thus, the soot production processes would be expected to be more repeatable than that in optical engines under similar operating conditions. On the other hand, the combustion process in optical engines is much more complicated because of the changing thermodynamic conditions, spray wall impingement and strong air-flow effects, which could result in strong cycle-to-cycle variations [16]-[18].

Most of previous studies focus on soot quantification with high sooting fuels [9][19]-[24] under relatively high sooting conditions, where soot formation takes place within each injection cycles. Pickett and Siebers [9] measured soot in diesel jets in HTHP by means of a point laser-extinction technique and laser-induced incandescence imaging. In this study, the ambient gas temperatures from 850 to 1300 K and the maximum KL value are higher than one for most operating conditions. The soot production of different biodiesels was studied by Zhang [20] and Xuan [24] by means of two-color method (2C) and a diffused back-illumination (DBI) extinction imaging technique, respectively. The soot maximum KL values in both literatures are also quite higher than one. Besides above literatures, a few works also focus on fully soot free combustion. Pickett and Siebers studied non-sooting combustion of diesel sprays in a HTHP vessel over a variety of operating conditions [25]. They concluded that this non-sooting combustion could be produced by means of small orifice nozzle, low ambient temperature and low oxygen concentrations. After that, Polonowski et al. investigated soot-free combustion strategies in a heavy-duty optical diesel engine with three injectors equipped with different number of nozzle holes [26]. Besides the conclusions from Pickett and Siebers, they also found that the re-entrainment of hot combustion products induced by wall impingement and proximity coupling induced by jet-to-jet spacing influence also plays important roles on in-cylinder soot formation. However, no information can be found for in-flame soot characterization under sooting/non-sooting critical conditions, namely threshold conditions where the soot can be produced or not be produced in the flame. With the development of advanced low temperature combustion (LTC) modes in CI engines, the in-flame soot production will become much less and the increase knowledge on in-flame soot quantification under such sooting/non-sooting critical conditions will be very helpful for these LTC mode improvement.

The aim of this paper is to improve the understanding for in-flame soot variation under sooting/non-sooting critical conditions by comparing two different optical techniques. The reasons for this strong soot variation will be figured out and the effects of ambient operating conditions on the soot variation will be studied. Additionally, the advantages and limitations of both optical techniques under such low sooting conditions will be compared. Consequently, n-dodecane under low sooting conditions, as well as a less sooting fuel, n-heptane, were selected to do the investigation in an adapted two-stroke optical diesel engine where a strong airflow exists because of the piston movement which could lead a strong cycle-to-cycle variation on fuel-air mixing. DBI and 2C techniques have been applied simultaneously to measure the instantaneous in-flame soot production (net result of soot formation and oxidation). In addition, the cylinder pressure is also recorded to assist the analysis.

Including the present introduction, this document is composed of four sections. The next section gives a detailed description about the experimental facility, soot optical diagnostics and the test plan investigated in this paper. In the third section, the methodology of in-cylinder soot characterization is presented. The last section summarizes some of the most important conclusions of this investigation.

2 Experimental tools and test plan

2.1 Test rig

An optically accessible single cylinder two-stroke engine with three-liter displacement, 15.6:1 compression ratio and low engine speed (500 rpm) has been used for these experiments, which is described in detail in [27]. A cylindrical combustion chamber is designed with a diameter of 45 mm. This chamber has one upper access for the fuel injector, and four lateral orthogonal accesses. One of them is used for the pressure transducer whereas the other three are equipped with optical windows with geometrical dimensions of 88 x 37 mm and 28 mm thick. The Cross-sectional view of cylinder head is shown in Fig. 1. During engine operation, the block temperature is controlled by an external heating-cooling system. The intake air temperature and pressure are controlled by electrical resistors and an air compressor respectively. An injection takes place every 30 cycles, which guarantees that there is no remaining residual gas from previous combustion cycles and the ambient conditions in the chamber are kept constant between consecutive repetitions. The fuels used in this paper were n-dodecane and n-heptane. Two common rail single-hole injectors fitted with nozzles with diameters 82 µm and 138 µm have been used in the experiments for n-dodecane and n-heptane, respectively. Thanks to the adequate cooling of the injector holder and the low injection frequency during operation, the nozzle tip temperature can be considered constant.

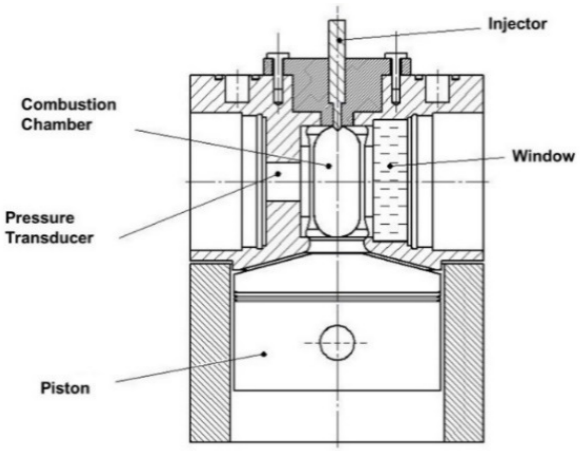

Fig. 1 Cross-sectional view of cylinder head

2.2 Optical techniques

Simultaneous high speed DBI and 2C measurements has been realized thanks to the arrangement of the optical setup as shown in Fig. 2. The optical setup, all optical components and camera settings are same with authors' previous literature[1]. Only some main principles are briefly stated here.

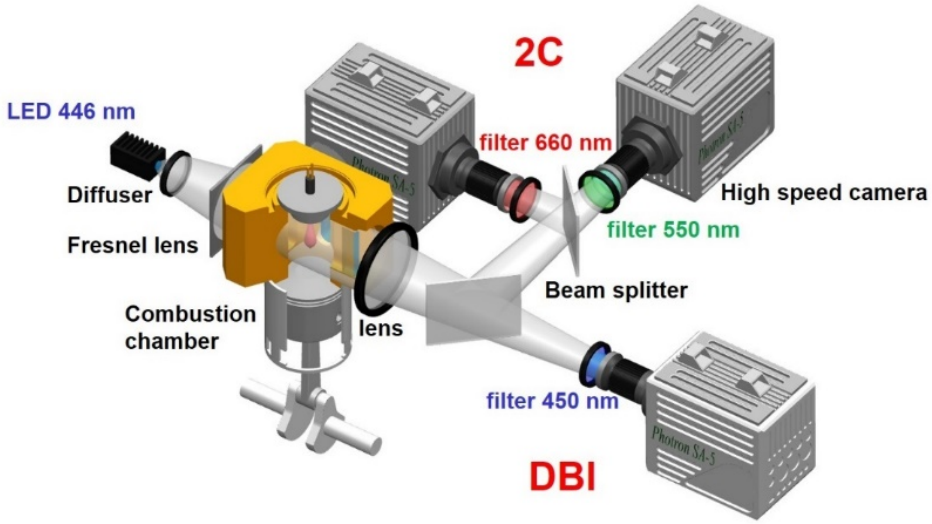

Fig. 2 optical arrangement

2.2.1 Diffused Back-illumination Extinction Imaging

A blue LED with was applied here as the light source to create high-output pulse light. A diffuser is placed in front of the LED to create a diffused Lambertian intensity profiles. After that, a Fresnel lens was mounted to magnify the visualization area to make it can cover the whole optical accesses. The distance between Fresnel lens and diffuser was kept a litter longer than the focus length of Fresnel lens in order to reduce the beam steering effects from vapor phase on extinction. On the collection side, the transmitted light of LED and the flame radiation are collected by a high-speed CMOS camera after passing through a spherical lens, a beam splitter and a corresponding bandpass filter. The DBI optical setup and all optical components are pretty similar compared to the ones in [2]. The only difference is the camera settings. Here, the exposure time of the camera was set to 6.62 ms with 264X640 pixels image resolution running at 35 kHz and the pixel/mm ratio is 7.71. The light intensity detected by the camera includes two parts: the transmitted LED light intensity and the flame intensity. Due to the use of an interference filter, the crosstalk of flame radiation into the DBI camera is minimized in the visible wavelength range. However, the flashing frequency of the LED was set as half of the camera frame rate to capture an image between every two successive LED pulses, so that flame luminosity can be quantified and this information used to get the correct transmitted LED light.

According to the Beer-Lambert law, the soot optical thickness (KL) was obtained after the correction.

$$\frac{I - I_f}{I_0} = \exp(-KL) \tag{1}$$

The pulse frequency of LED was triggered as half as camera framerate, so that both LED on and off images are alternatively recorded. I is the sum of the transmitted LED intensity and the flame luminosity as recorded by the DBI camera for a LED-on image, I_f is the intensity of the flame acquired for a LED-off image, K is the dimensional extinction coefficient and L is the path length of the light beam through the soot cloud. I_0 is the incident radiation, as obtained from images before start of injection. The detailed information of the processing methodology to obtain the soot KL values can be referenced from[2]. Besides, the sum of soot mass (m_{soot}) along the line-of-sight at each pixel was derived from using an assumed density of 1.8 g/cm^3 for soot (ρ_{soot})[28][29]:

$$m_{soot} = \rho_{soot} KL \frac{\lambda_I}{k_e} \times \text{ pixel area} \quad (2)$$

where λ_I is the extinction wavelength and k_e is the dimensionless extinction coefficient. The total soot mass is then the sum of all pixel specific values over the entire image.

2.2.2 Two-color method

Besides extinction, the soot radiation intensity was directed into another two high-speed cameras by means of two beam splitters. Each of these cameras was equipped with a bandpass filter centered at 550 nm and 660 nm respectively. In order to make a comparison between DBI and 2C results at the same time during the same injection, all three cameras have been synchronized and image resolutions were also kept same.

The 2C assumes that the flame radiation (with uniform spatial temperature and soot distributions) depends on the wavelength, the temperature and the amount of soot. The soot radiance I_{soot} can be expressed as follows:

$$I_{soot} = \varepsilon \cdot I_b \quad (2)$$

where the black-body radiance (I_b) can be written from Planck's law:

$$I_b(\lambda, T) = \frac{1}{\lambda^5} \frac{c_1}{[\exp\left(\frac{c_2}{\lambda T}\right) - 1]} \quad (3)$$

and the emissivity ε can be obtained using the empirical correlation developed by Hottel and Broughton (1932)[30]:

$$\varepsilon(KL, \lambda) = 1 - \exp(\frac{-KL_{2C}}{\lambda^{\alpha}}) \quad (4)$$

where c_1 and c_2 are constants, $c_1 = 1.1910439 \times 10^{-16}$ w m^{2}sr^{-1} and $c_2 = 1.4388 \times 10^{-2}$ mk.

KL_{2C} is the optical thickness calculated from 2C method. In order to transform grey levels into radiance values, calibration curves have been obtained by means of a tungsten-ribbon calibration lamp (Osram Wi17G), which was located at the same distance from the 2C cameras as the distance between the cameras and flame in the combustion chamber.

2.2.3 OH* chemiluminescence

Even though it is not shown in Fig. 2, the flame lift-off length (LOL) was also quantified for n-dodecane cases by means of the recording of OH* chemiluminescence radiation. An Andor Solis iStar ICCD intensified camera equipped with a 100 mm focal length f/2 UV objective and a 310 nm interference filter (FWHM = 10 nm) was used. Only one image per injection event was recorded from 4 ms to 5 ms after start of energizing (ASOE) with a pixel/mm ratio of 10.9.

2.3 Test plan

The investigated operating conditions are summarized in Tab.1. This test plan includes 4 operating conditions (2 operating conditions for each fuel) that have been denoted as high temperature (HT), low temperature (LT) and medium temperature (MT) conditions and three injection pressures were carried out for each of them. To determine the intake pressure and temperature values required to achieve the target TDC conditions, an accurate characterization of the engine has been

performed. Thermodynamic conditions inside the cylinder have been calculated from measured pressure, using a first-law thermodynamic analysis [31]. In order to do normalized analysis under different entrainment conditions, an equivalent diameter $d_{eq} = d_0\sqrt{\frac{\rho_f}{\rho_a}}$ will be applied in later section according to the classic definition in the literature [32][33]. A long injection energizing time was set as 4 ms at every operating point, which results in an injection duration around 5 ms, approximately. For the experiments of n-dodecane and n-heptane, 40 injections and 30 injections have been recorded respectively at each operating condition, respectively.

Tab. 1 Test conditions.

Operating conditions	Fuel	P_{inj} [bar]	T_a [K]	ρ_a [kg/m^3]	O_2 [%]	d_{eq} [mm]	COMMENTS
HT	n-dodecane (C12) n-heptane (C7)	500/1000/1500	**870**	22.8 (C12) 21.2 (C7)	21	0.471 0.756	High Temperature
LT	n-dodecane (C12)	500/1000/1500	780	22.8	21	0.471	Low Temperature
MT	n-heptane (C7)	500/1000/1500	826	21.2	21	0.756	Medium Temperature

3 Results and discussion

3.1 Probability of sooting cycles

A sequence of DBI and 2C radiation images (660 nm) of n-dodecane from 9 injections (out of 40) at 3200 μs ASOI (after start of injection) under LT500 (500 represents that injection pressure is 500 bar) condition are presented in Fig. 3 to show soot cycle-to-cycle variations. The fuel was injected vertically from top to the bottom of the optical window. A strong extinction near injector can be observed from DBI images which is mainly caused by Mie-scattering from fuel liquid droplets. From Fig. 3 both techniques present a good agreement on the soot location and soot amount. A huge cycle-to-cycle variation can be observed from both techniques, where a strong soot extinction and radiation signal can be observed in the injection of second, third and eighth columns, while no soot can be detected in the injections of fifth and sixth columns. The apparent heat release rate (AHRR) is derived according to the first law of thermodynamics from cylinder pressure trace, which is recorded from a high-speed piezoelectric transducer installed in the combustion chamber. The corresponding AHRR to the injection cycles presented in Fig. 3 and averaged one over 40 injection cycles are shown in Fig. 4. It can be observed that the AHRR evolution is quite repeatable. Furthermore, the ignition delays are also quite repeatable over total injection cycles where the standard deviation of ignition delay is just 0.05 ms. In summary, it indicates the soot cycle-to-cycle variations are not mainly caused by ignition delay and heat release variations.

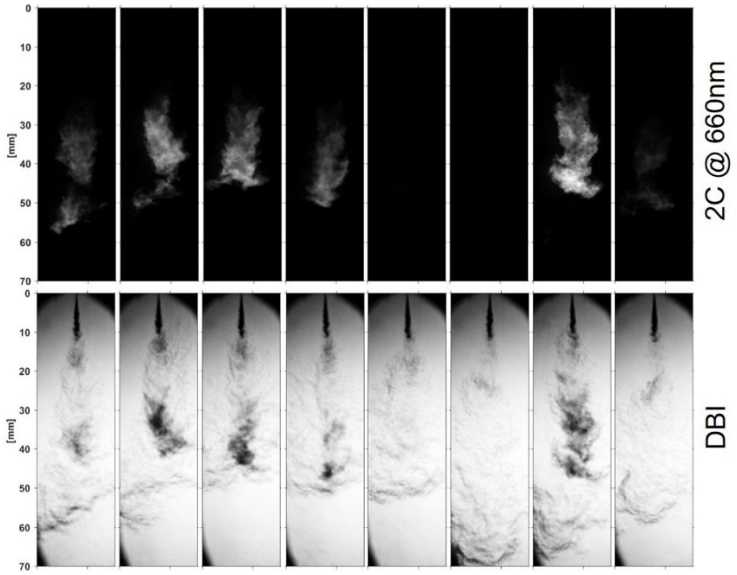

Fig. 3 One example of soot cycle-to-cycle variations at 3200 μs ASOI (C12, LT500).

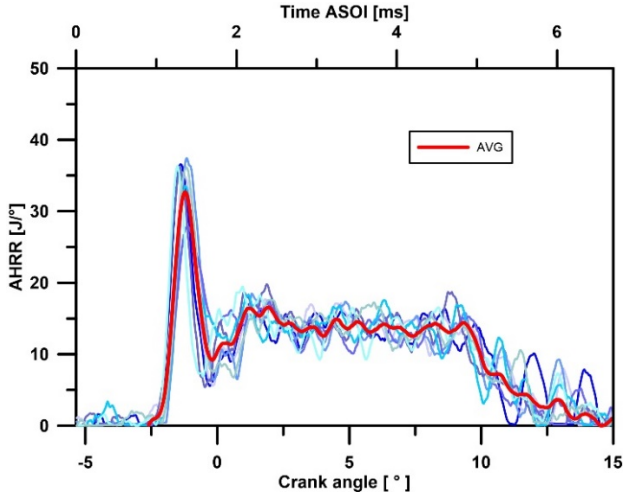

Fig. 4 Corresponding AHRR to Fig. 3 and averaged one (red curve) over 40 cycles (C12, LT500).

A procedure for the quantification of the sooting/non-sooting transition has been developed based upon 2C radiation images at wavelength of 660 nm, which the signal-to-noise ratio is higher than that of 550 nm. Radiation occurs whenever soot is present at a high-enough temperature, and it is not subjected to beam-steering limitations in the lower range, as is the case of DBI. For each individual injection cycle, the digital values at each pixel (I_{pixel}) within each frame are integrated to get the time evolution as shown in Fig. 5 (a). After that, one single total radiation digital value (I_{cycle}) is derived by integrating the area below this time evolution, as shown in the following equation.

$$I_{cycle} = \iint I_{pixel} dn_{pixel} dn_{frame} \quad (5)$$

where the n_{pixel} is the pixel number within each frame and n_{frame} is the frame number recorded for each injection. Thus, the total integrated radiation digital values with cycle variation is obtained, as shown in Fig. 5 (b). Finally, one threshold with 1.2 times of averaged background noise multiplying total frame of per injection was selected to quantify sooting/non-sooting combustion for all operating cases. As observed in Fig. 5 (b), the cycles with star markers above the red threshold line are defined as sooting cycles. It could be argued that soot radiation intensity is more governed by local temperature and it might not be suitable to represent soot amount. Thus, the integrated total soot mass over total frames of each cycle is also

derived from DBI images and the relationship between total soot mass and total soot radiation intensity is presented in Fig. 6. It can be observed that soot amount increases with increasing radiation intensity roughly linearly. On the other hand, the difficulty to remove beam-steering interference on extinction for DBI technique has to be considered, which could bring some uncertainties on soot quantification, especially for lower sooting cases. Finally, radiation images have been used for this sooting/non-sooting quantification instead of using DBI images.

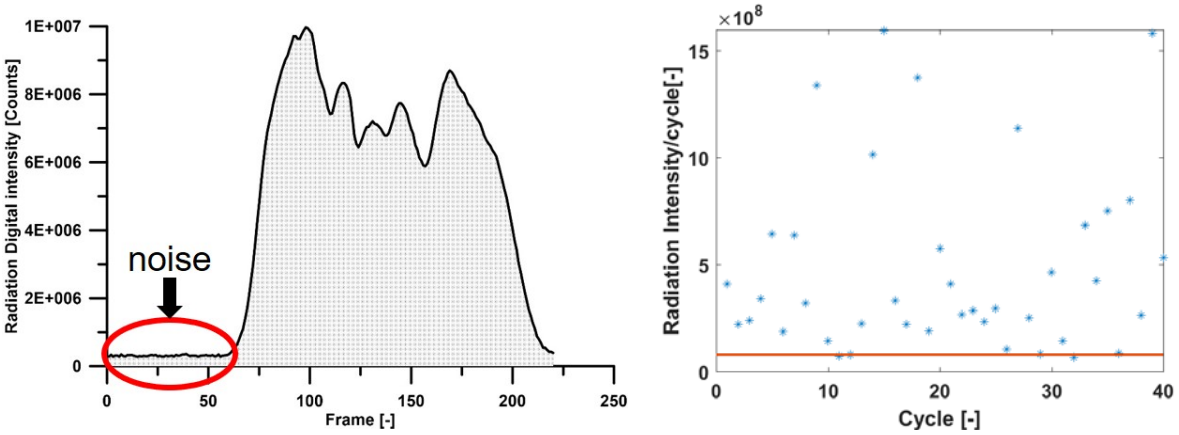

(a) Integrated radiation digital values with frame evolution for a single injection cycle (b) total Integrated radiation digital values with cycle variation

Fig. 5 Procedure for quantification of the sooting/non-sooting cycles with radiation images (C12, LT500).

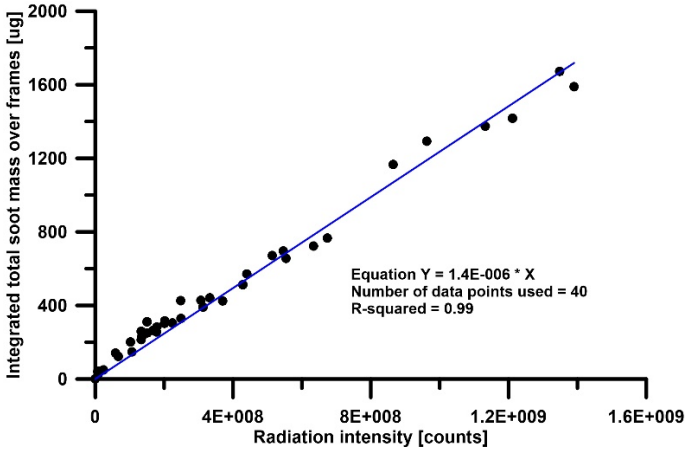

Fig. 6 Relationship between total soot radiation and total soot mass of each cycle of n-dodecane under LT500 operating condition.

Based on Fig. 5, the probabilities of sooting cycles, defined as the number of cycles where soot occurs divided by the total repetitions, are summarized in Fig. 7 for both fuels under all operating conditions. Apparently, the probability of sooting cycles increases with higher ambient temperature, higher ambient density and lower injection pressure. It is consistent with the soot amount trend to operating conditions when soot production happens in all repetitions [9]. One interesting thing can be observed that this probability of n-heptane is lower than that of n-dodecane under HT conditions, even though the nozzle diameter used for n-heptane is much bigger and the axial KL value is also a little higher (Fig.12).

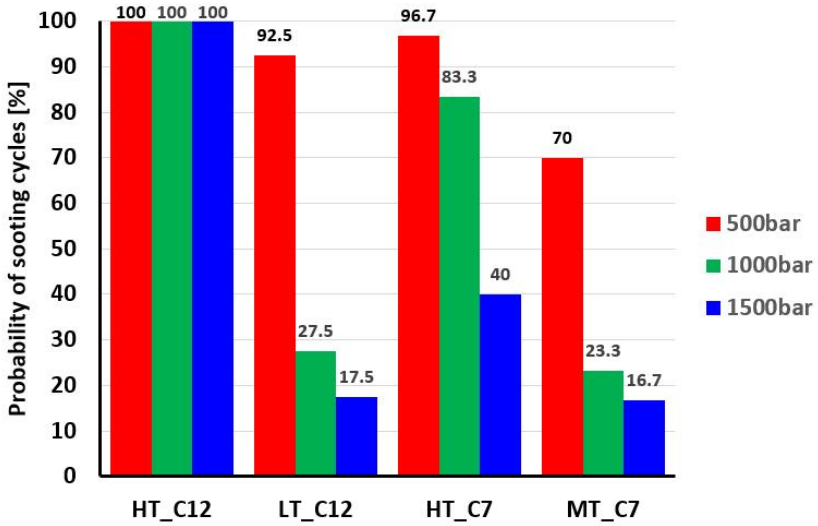

Fig. 7 Probability of sooting cycles for all operating conditions

One possibility of this sooting/non-sooting transition is that the in-cylinder airflow caused by piston movement, which has a quite strong cycle-to-cycle variation as characterized by PIV in the same engine presented in reference [16][34]. It was shown in [34] that the standard deviation of airflow velocity reaches local values of the same order of magnitude as the corresponding average velocity. As shown in [16] and Fig. 4, the airflow does not create a significant influence on ignition delay variation because the ignition locations are usually located at spray upstream near injector where the airflow velocity is very slow. However, it indeed has a strong influence on flame downstream. Fig. 8 presents a comparison between spray axial velocity (which is derived from a 1D spray model [35][36]) and ambient airflow axial velocity (which is derived from previous PIV measurement [16]) under non-reacting conditions. It can be observed from Fig. 8 that the airflow velocity (~ 5 m/s) at spray tip is almost negligible compared to spray tip velocity (~ 60 m/s) at the beginning of fuel injection (-4° ATDC). However, the airflow axial velocity becomes much more important when the spray penetrates farther than 40 mm at -2° ATDC (more than 25% of spray tip velocity). As a consequence, the strong cycle-to-cycle variation on airflow velocity will bring a significant influence on fuel-air mixing. What's more, it can be speculated that the variation of airflow can also influence fuel-air mixing of reacting spray, as well as soot production.

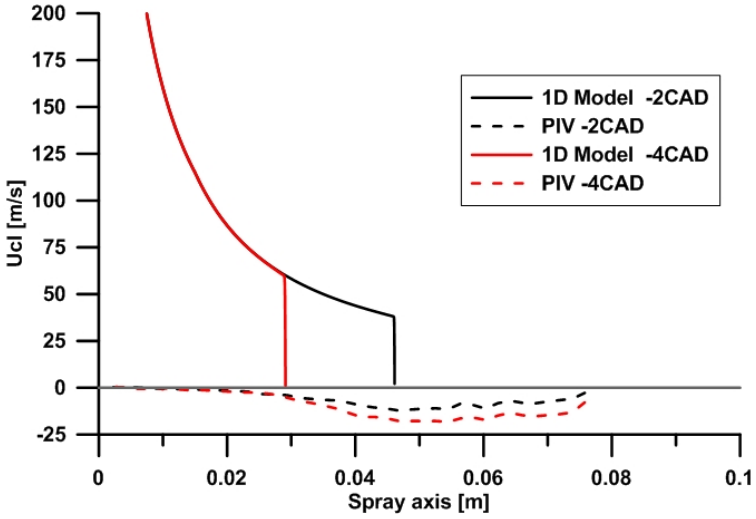

Fig. 8 Spray axial velocity (solid lines) and ambient airflow axial velocity (dashed lines). (T_a =760 K, ρ_a =19.3 kg/m^3)

Furthermore, the airflow also has a strong influence on flame lift-off length variation. The OH* images and corresponding

LOL values of n-dodecane of from 6 injections under LT500 condition are presented in Fig. 9. It can be found the LOL can range from 10.3 mm to 24.2 mm. This could be mainly caused by strong cycle-to-cycle variation of backward flow of hot burned gas. Fuyuto et al. [38][39] also observed similar phenomenon in engine combustion chamber with multiple-hole injectors.

It is known that there is a strong relationship between flame LOL and soot production [9]. The LOL and corresponding cross-sectional average equivalence ratio at LOL ($\bar{\Phi}_{\mathrm{H}}$) of n-dodecane under all operating conditions are shown in Fig. 10, where the error bars represent cycle-to-cycle variation. $\bar{\Phi}_{\mathrm{H}}$ is estimated based on the expressions as follows, which is referenced from [9][25][26].

$$\bar{\Phi}_{\mathrm{H}} = \frac{2 \cdot (A/F)_{st}}{\sqrt{1 + 16 \cdot \left(\frac{H}{x^{+}}\right)^{2} - 1}} \tag{6}$$

where $(A/F)_{st}$ is the stoichiometric air-furl ratio by mass for a given fuel, H is the value of LOL. x^{+} is a characteristic length scale for the fuel jet which is defined as following equation:

$$x^{+} = \sqrt{\frac{\rho_f}{\rho_a}} \frac{\sqrt{C_a} \cdot d_0}{a \cdot \tan(\theta/2)} \tag{7}$$

where C_a is the orifice area contraction coefficient, a is a constant with a value of 0.75, and $\theta/2$ is the jet spreading half-angle.

As proved in [25][26], a soot free combustion will occur when $\bar{\Phi}_{\mathrm{H}} < 2$. Two different $\bar{\Phi}_{\mathrm{H}}$ values are presented in Fig. 10 for each operating condition with two limit positions of LOL ($\mathrm{LOL} \mp$ std). It can be found that the strong variation of LOL also leads to a strong influence on $\bar{\Phi}_{\mathrm{H}}$ values. The up limits of $\bar{\Phi}_{\mathrm{H}}$ values of LT1000 and LT1500 cases are smaller than 2, consequently, some non-sooting combustion cycles takes place. On the other hand, the up limits of $\bar{\Phi}_{\mathrm{H}}$ values of the other four conditions are all greater than 2, thus, the soot will be produced within all cycles. It is consistent with the probability of sooting cycles as shown in Fig. 7. It needs to be pointed out that the OH* measurements were not carried out simultaneously with soot measurements, which could be the reason for this non-perfect consistency on LT500 between Fig. 7 and Fig. 10.

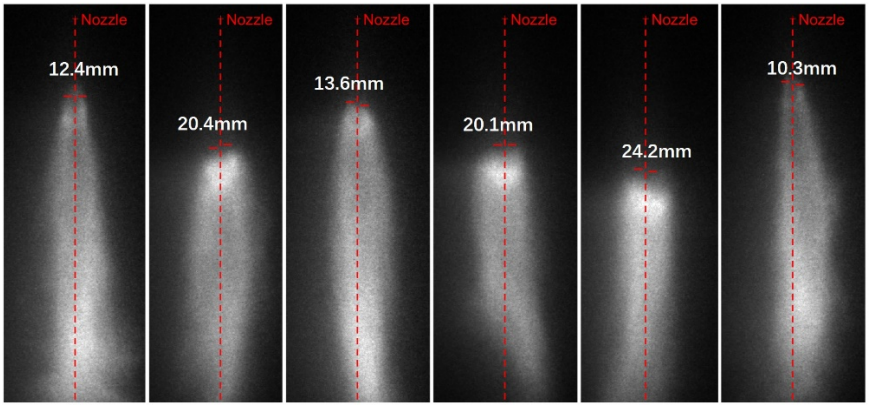

Fig. 9 One example of OH* images of six injections under LT500 condition with fuel of n-dodecane

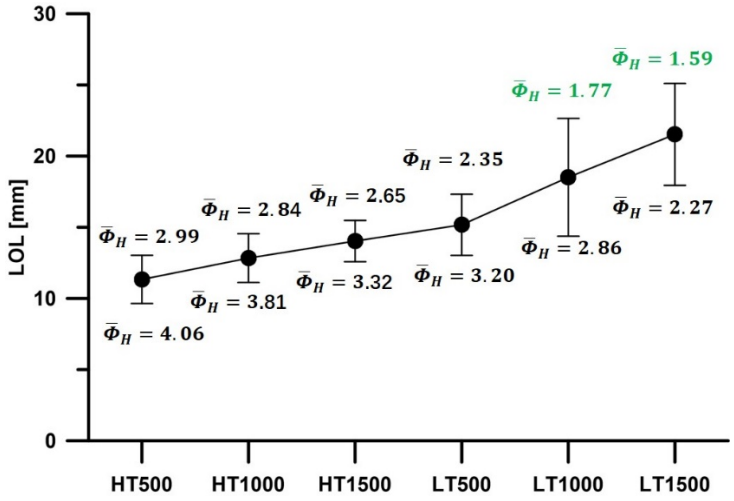

Fig. 10 LOL and corresponding $\bar{\Phi}_H$ of n-dodecane. Error bars represent cycle-to-cycle variation.

3.2 Soot quantification

In order to make parametric comparisons for in-flame soot production, averaged KL values over all repetitions are obtained from DBI images. The averaged axial KL value comparisons (at 3800 μs ASOI) of three injection pressures under LT and MT conditions for n-dodecane and n-heptane respectively are shown in Fig. 11. The distance away from the nozzle orifice is normalized with the equivalent diameter. In general, the trend of soot production with injection pressure of both fuels is consistent with previous literatures, where the KL value increases with lower injection pressure because of shorter LOL and longer residence time [9][37]. However, the difference of KL values between LT1000 and LT1500 cases of n-dodecane is quite small. With present setup, beam steering still exists because of the imperfect Lambertian light source, which determines the lower KL detection limit. Fig. 12(a) presents the axial KL values averaged over non-sooting cycles for the fuel of n-dodecane, where the light extinction is mainly caused by beam steering. Fig. 12(b) presents one example of comparison for axial KL values averaged over all cycles and non-sooting cycles under LT1000 condition. It can be found from Fig. 12(b) that under such low sooting conditions (KL <0.2) it is beyond the lower KL detection limit of DBI technique, where the extinction caused by beam steering is almost equal to the KL value averaged over all cycles. As a consequence, even though it is supposed the axial KL value of LT1000 is higher than that of LT1500 because of shorter LOL and longer residence time, the difference can be hardly distinguished.

As observed for those quite low sooting conditions, both soot amount and soot radiation intensity are quite low, which could result in a low signal-to-noise ratio and high uncertainties on DBI and 2C results. As a consequence, in order to make a comparison between DBI and 2C to check the sensitivity of both techniques to operating conditions in following analysis, the KL values are calculated based on images averaged over only sooting cycles to increase the signal-to-noise ratio.

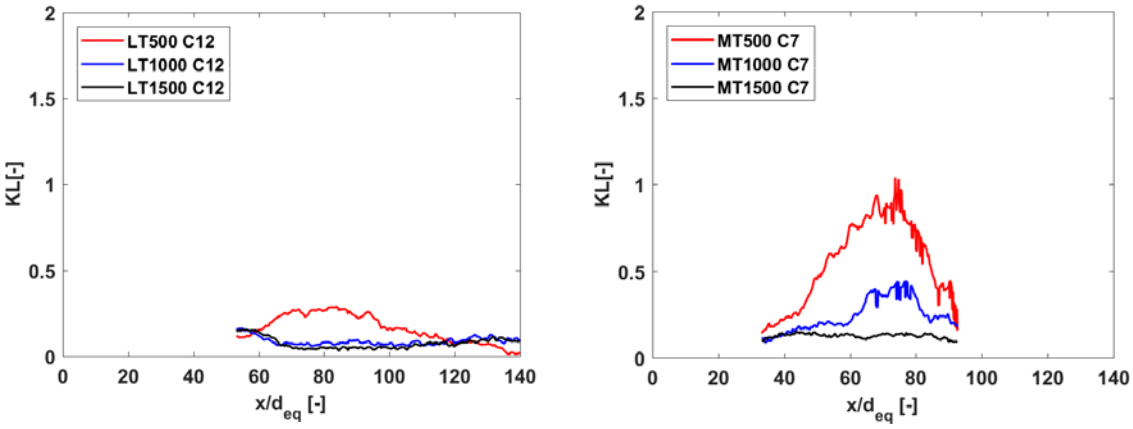

(a) LT, n-dodecane (b) MT, n-heptane

Fig. 11 Averaged axial DBI-derived KL value of three injection pressures over total cycles (at 3800 μs ASOI).

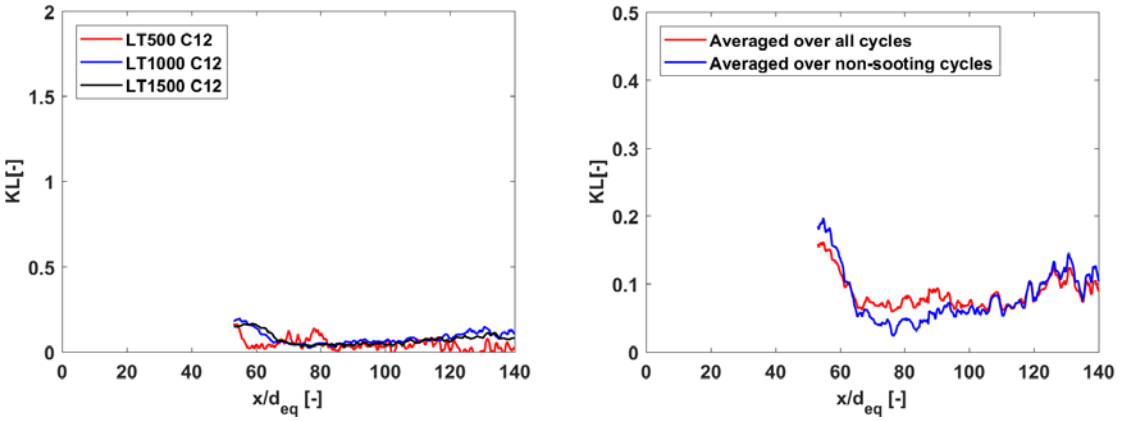

(a) Axial KL values averaged over sooting cycles (b) Axial KL values under LT1000 conditions

Fig. 12 Beam steering effects on KL values of n-dodecane (at 3800 μs ASOI, LT condition).

As for DBI technique, the extinction caused by scattering is negligible according Rayleigh-Debye-Gans theory [1][40]. Thus, the soot absorptivity α_{λ_I} under extinction wavelength λ_I can be obtained as follows:

$$\alpha_{\lambda_I} = 1 - \tau = 1 - \exp(-KL_I) \tag{8}$$

where τ is transmissivity.

According to Kirchhoff law, under thermal equilibrium the absorptivity equals emissivity, as shown below

$$1 - \exp(-KL_I) = 1 - \exp(\frac{-KL_{2C}}{\lambda_I^{\alpha}}) \tag{9}$$

where α is the dispersion exponent and it is taken as 1.39 according to [3]. As a consequence, the relationship of the optical thickness between DBI and 2C can be expressed as follows:

$$KL_I = 3.034 \cdot KL_{2C} \tag{10}$$

In order to make the KL values from these two techniques more comparable, the KL_{2C} value will be converted into DBI scale according to Eq.(10) . One thing needs to be pointed out here that the soot KL value from both DBI and 2C techniques are calculated over sample-averaged images, instead of instantaneous images.

Fig. 13 shows axial KL values from both techniques, as well as the axial soot temperature from 2C, where two cases under relatively high sooting and low sooting conditions are presented for each fuel. It can be observed from Fig. 13(c) that both techniques present a pretty good agreement on the soot amount quantification when the maximum KL value is close to 1, which is consistent with the findings presented in [1]. This means that the uncertainty caused by soot signal self-absorption can be negligible under such low sooting conditions. However, an apparent difference appears between two techniques when the KL value becomes smaller (Fig. 13(a)) where the KL of 2C is higher than that of DBI and the difference becomes bigger with continuous decreasing KL value (Fig. 13(b) and Fig. 13(c)). It is opposite with the findings in [1] where the KL of DBI is much higher than that of 2C due to the strong signal self-absorption effects on 2C, which is obtained under high sooting conditions where the maximum KL value is much higher than 1. One possibility is that the sensitivity of light extinction of DBI under such low sooting conditions is not as strong as high sooting conditions which could be caused by more important role of light diffraction when it passes through tiny soot particles, i.e. beam-steering effects. Consequently, the transmitted light would be higher and the calculated KL value would be smaller than the real one. In general, the soot temperature follows the same trend with the results from previous research, i.e. temperature increases with spray axis until the flame tip.

In summary, according to the findings in present paper and our previous research [1], both techniques present their advantages and limitations on Diesel spray in-flame soot quantification.

- When soot production is too high (KL_{max} >>1), the results from DBI is more senstive to soot amount than that of 2C.
- When KL_{max} is close to 1, DBI and 2C present a good agreement.
- When soot production is too low (KL_{max} <0.2), it beyonds the detection limit of present DBI setup.

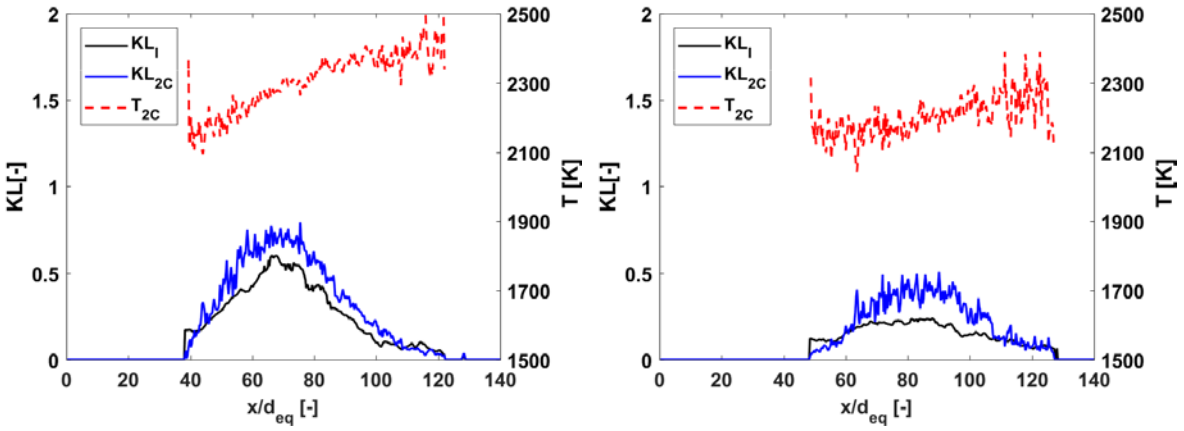

(a) HT500, C12 (probability of sooting cycles = 100%) (b) LT500, C12 (probability of sooting cycles = 92.5%)

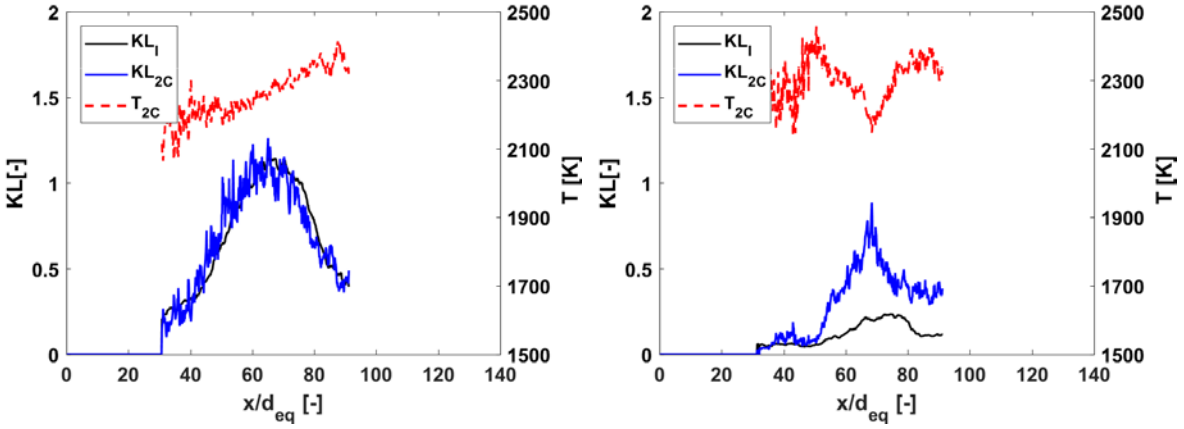

(c) HT500, C7 (probability of sooting cycles = 96.7%) (d) MT1000, C7 (probability of sooting cycles = 23.3%)

Fig. 13 Axial soot KL value and soot temperature at 3800 μs ASOI. Solid blue lines represent KL value from 2C, Solid black lines represent KL value from DBI, red dashed lines represent soot temperature from 2C.

4 Conclusions

A methodology was implemented to quantify the in-flame soot production of Diesel spray under sooting/non-sooting critical conditions. All the measurements were realized in a single cylinder two-stroke optical engine which was equipped with a single-hole injector. The fuel selected here were n-dodecane and n-heptane and the soot measurements were carried out by means of DBI and 2C simultaneously. The following conclusions were reached in this study:

1) Within this study, the soot production presents a quite strong cycle-to-cycle variation. However, the in-cylinder heat release rate is quite repeatable. One criterium based on radiation images was defined to quantify sooting or non-sooting cycles. The probability of sooting cycles increases with higher ambient temperature, higher ambient density and lower injection pressure.
2) The strong cycle-to-cycle variations of soot production are mainly caused by significant fluctuations on flame lift-off length which could be caused by the strong variation of in-cylinder flow. At least it has been proved under optical engine environment tested.
3) The trend of averaged soot KL value with injection pressure under such low sooting conditions is consistent with previous research. However, the present DBI setup is not able to quantify soot amount when the KL value is reaching the DBI lower KL detection limit determined by beam-steering.
4) Under studied operating conditions, DBI and 2C techniques present a pretty good agreement on soot amount quantification when the maimum KL value is close to 1 where soot signal self-absorption issues of 2C is almost negligible. However, KL of 2C is higher than that of DBI when the soot amount become less and the difference becomes bigger with continuous decreasing KL value

Acknowledgements

This study was partially funded by the Natural Science Foundation of China (No. 51876083), China Postdoctoral Science

Foundation (2018M642176) and High-tech Research Key laboratory of Zhenjiang (SS2018002).

Reference

[1] Skeen S., Manin J., Pickett L., Cenker E., et al.， A progress review on soot experiments and modeling in the Engine Combustion Network (ECN)， SAE International Journal of Engines, 9 (2016) 883-898, https://doi.org/10.4271/2016-01-0734.

[2] Pastor, J., Garcia-Oliver, J., García A., Xuan T., Soot Quantification of Single-Hole Diesel Sprays by Means of Extinction Imaging, SAE International Journal of Engines, 8(2015) 2068-2077, https:// doi:10.4271/2015-24-2417.

[3] Pastor J., Garcia-Oliver, J., García A., Micó C., et al., Application of optical diagnostics to the quantification of soot in n-alkane flames under diesel conditions, Combustion and Flame, 164 (2016) 212-223, https://doi.org/10.1016/j.combustflame.2015.11.018

[4] Jeon J., Park S., Effects of pilot injection strategies on the flame temperature and soot distributions in an optical CI engine fueled with biodiesel and conventional diesel, Applied Energy,160 (2015) 581-591, https://doi.org/10.1016/j.apenergy.2015.09.075

[5] Zhang, Y., Zhang, R., Rao, L., Kook, S., A Comparison between In-Flame and Exhaust Soot Nanostructures in a Light-Duty Diesel Engine, SAE Technical Paper 2017-01-0710, 2017 https://doi.org/10.4271/2017-01-0710.

[6] Kamimoto T., Uchida N., Aizawa T., Kondo K., et al., Diesel flame imaging and quantitative analysis of in-cylinder soot oxidation, International Journal of Engine Research, 18(2016) 422 – 435, https://doi.org/10.1177/1468087416629282

[7] Musculus M., Singh S., Reitz R., Gradient effects on two-color soot optical pyrometry in a heavy-duty DI diesel engine. Combustion and flame, 153 (2008) 216–227, https://doi.org/10.1016/j.combustflame.2007.10.023

[8] Dumitrescu C., Mueller C., Kurtz E., Investigation of a tripropylene-glycol monomethyl ether and diesel blend for soot-free combustion in an optical direct-injection diesel engine, Applied Thermal Engineering, 101 (2016) 639–646, https://doi.org/10.1016/j.applthermaleng.2015.12.068

[9] Pickett L., Siebers D., Soot in diesel fuel jets: effects of ambient temperature, ambient density, and injection pressure. Combustion and Flame, 138 (2004) 114-135, https://doi.org/10.1016/j.combustflame.2004.04.006

[10] Gehmlich R.K., Mueller C.J., Ruth D.J., Nilsen C.W., et al., Using ducted fuel injection to attenuate or prevent soot formation in mixingcontrolled combustion strategies for engine applications, Applied energy, 226 (2018) 1169–1186, https://doi.org/10.1016/j.apenergy.2018.05.078

[11] Bardi, M., Bruneaux, G., Nicolle, A., Colin, O., Experimental Methodology for the Understanding of Soot-Fuel Relationship in Diesel Combustion: Fuel Characterization and Surrogate Validation, SAE Technical Paper 2017-01-0721, 2017, https//:doi:10.4271/2017-01-0721.

[12] Mueller C., Nilsen C., Ruth D., Gehmlich R., et al., Ducted fuel injection: A new approach for lowering soot emissions from direct-injection engines, Applied energy, 204(2017)206-220, https://doi.org/10.1016/j.apenergy.2017.07.001

[13] Westlye Fredrik R., Penney Keith, et al, Diffuse back-illumination setup for high temporally resolved extinction imaging, Applied Optics, 56 (2017) 5028-5038.

[14] Manin J, Pickett L., Skeen S., Two-Color Diffused Back-Illumination Imaging as a Diagnostic for Time-Resolved Soot Measurements in Reacting Sprays. SAE Int. J. Engines, 6(2013)1908-1921, https://doi.org/10.4271/2013-01-2548

[15] Moiz A., Ameen M, Lee s. Som S., Study of soot production for double injections of n-dodecane in CI engine-like conditions, Combustion and Flame 173 (2016) 123–131,https://doi.org/10.1016/j.combustflame.2016.08.005

[16] Pastor, J., García J.M., Garcia, A., Zhong, W. et al., An experimental study on Diesel spray injection into a non-quiescent chamber, SAE Int. J. Fuels Lubr.10 (2017) , https://doi.org/10.4271/2017-01-0850.

[17] Kyrtatos, P., Zivolic, A., Brueckner, C., Boulouchos, K., The Effect of Cycle-to-Cycle Variations on the NOx-SFC Tradeoff in Diesel Engines under Long Ignition Delay Conditions, SAE Int. J. Engines 10 (2017)2451-2460, https://doi.org/10.4271/2017-24-0100

[18] Bizon K., Continillo G., Mancaruso E., Merola S.S., et al., POD-based analysis of combustion images in optically accessible engines, Combustion and Flame, 157 (2010) 632–640, https://doi.org/10.1016/j.combustflame.2009.12.013

[19] Jeon J., Park S., Effect of injection pressure on soot formation/oxidation characteristics using a two-color photometric method in a compression-ignition engine fueled with biodiesel blend (B20), Applied Thermal Engineering 131 (2018) 284–294, https://doi.org/10.1016/j.applthermaleng.2017.12.005

[20] Zhang J., Jing W., Roberts W., Fang T., et al., Soot temperature and *KL* factor for biodiesel and diesel spray combustion in a constant volume combustion chamber, Applied energy, 107 (2013) 52–65, https://doi.org/10.1016/j.apenergy.2013.02.023

[21] López J., Martín J., García A., Villalta D., et al., Implementation of two color method to investigate late cycle soot oxidation process in a CI engine under low load conditions, Applied Thermal Engineering 113 (2017) 878–890, https://doi.org/10.1016/j.applthermaleng.2016.11.095

[22] Jung Y., Park S., Bae C., Effect of oxygen concentration on highly diluted charge compression ignition combustion in an optical engine, Applied Thermal Engineering 90 (2015) 538-550, https://doi.org/10.1016/j.applthermaleng.2015.07.049

[23] García A., Monsalve-Serrano J., Heuser B., Jakob M., et al., Influence of fuel properties on fundamental spray characteristics and soot emissions using different tailor-made fuels from biomass, Energy Conversion and Management 108 (2016) 243–254, https://doi.org/10.1016/j.enconman.2015.11.010

[24] Xuan T., Cao J., He Z., Wang Q., et al., A study of soot quantification in diesel flame with hydrogenated catalytic biodiesel in a constant volume combustion chamber, Energy 145 (2018) 691-699, https://doi.org/10.1016/j.energy.2017.12.106

[25] Pickett, L., Siebers, D., Non-Sooting, Low Flame Temperature Mixing-Controlled DI Diesel Combustion, SAE Technical Paper 2004-01-1399, 2004 https://doi.org/10.4271/2004-01-1399.

[26] Polonowski, C., Mueller, C., Gehrke, C., Bazyn, T. et al., An Experimental Investigation of Low-Soot and Soot-Free Combustion Strategies in a Heavy-Duty, Single-Cylinder, Direct-Injection, Optical Diesel Engine, SAE Int. J. Fuels Lubr. 5(2012)51-77 https://doi.org/10.4271/2011-01-1812.

[27] Bermúdez, V., García, J., Juliá, E., Martínez, S., Engine with Optically Accessible Cylinder Head: A Research Tool for Injection and Combustion Processes, SAE Technical Paper 2003-01-1110, 2003, https://doi.org/10.4271/2003-01-1110

[28] Skeen, S., Yasutomi, K., Cenker, E., Adamson, B. et al., Observations of Soot Optical Property Characteristics Using High-Speed, Multiple Wavelength, Extinction Imaging in Heavy-Duty Diesel Sprays, SAE Technical Paper 2018-01-0233, 2018, https://doi:10.4271/2018-01-0233.

[29] Desantes J., García-Oliver J., García A., Xuan T., Optical study on characteristics of non-reacting and reacting diesel spray with different strategies of split injection, International Journal of Engine Research, May 13, 2018, https://doi.org/10.1177/1468087418773012

[30] Hua Zhao, N. Ladommatos, Engine combustion instrumentation and diagnostics. Warrrendale PA: Society of Automotive Engineers, 2001

[31] Nerva J. G., An assessment of fuel physical and chemical properties in the combustion of a Diesel spray, PhD Thesis, 2013

[32] Ricou F, Spalding D, Measurements of entrainment by axisymmetrical turbulent jets, J. Fluid Mech. 11 (1961) 21, https://doi.org/10.1017/S0022112061000834

[33] M.W. Thring , M.P. Newby , Combustion length of enclosed turbulent jet flames, Symp. Combust. 4 (1953) 789–796

[34] Reche C. M., Development of measurement and visualization techniques for characterization of mixing and combustion processes with surrogate fuels, PhD Thesis, 2015

462 [35] Pastor J., López J., García J., Pastor J., A 1D Model for the Description of Mixing-Controlled Inert Diesel Sprays,
463 Fuel, 87 (2008) 2871-2885
464 [36] Desantes J., Pastor J., García J., Pastor J., A 1D Model for the Description of Mixing-Controlled Reacting Diesel
465 Sprays, Combust. Flame 156 (2009) 234-249
466 [37] Xuan T., Optical investigation on diesel spray dynamics and in-flame soot formation. PhD Thesis, 2017
467 [38] Fuyuto T., Hattori Y.. Backward Flow of Hot Burned Gas Surrounding High- Pressure Diesel Spray Flame from Multi-
468 hole Nozzle. SAE International Journal of Engines, 2015, https://doi.org/10.4271/2015-01-1837
469 [39] Fuyuto T., Hattori Y., Yamashita H., Toda N. et al., Set-off length reduction by backward flow of hot burned gas
470 surrounding highpressure diesel spray ame from multi-hole nozzle. International Journal of Engine Research,
471 18(2017)173-194, https://doi.org/10.1177/1468087416640429
472 [40] Koylu U. O., Faeth G. M. Optical properties of overfire soot in buoyant turbulent diffusion flames at long residence
473 times. Journal of heat transfer, 116(1994):152-159, https:// doi:10.1115/1.291084